Fluence correction factors for graphite calorimetry in a low-energy clinical proton beam: I.

Analytical and Monte Carlo simulations

Fluence correction factors for graphite calorimetry in a low-energy clinical proton beam: I. Analytical and Monte Carlo simulations

H Palmans[1,9]**, L Al-Sulaiti**[1,2,10]**, P Andreo**[3]**, D Shipley**[1]**, A Lühr**[4,5]**,
N Bassler**[5]**, J Martinkovič**[6]**, J Dobrovodský**[6]**, S Rossomme**[7]**,
R A S Thomas**[1] **and A Kacperek**[8]

[1] Acoustics and Ionising Radiation Division, National Physical Laboratory, TW11 0LW Teddington, UK
[2] Department of Physics, University of Surrey, GU2 7XH Guildford, UK
[3] Division of Medical Radiation Physics, Stockholm University at Karolinska University Hospital, SE-171 76 Stockholm, Sweden
[4] Department of Experimental Clinical Oncology, Aarhus University Hospital, DK-8200 Aarhus C, Denmark
[5] Department of Physics and Astronomy, Aarhus University, DK-8000 Aarhus C, Denmark
[6] Slovenský Metrologický Ústav, Centrum Ionizujúceho Žiarenia, SK-84255 Bratislava, Slovak Republic
[7] Université Catholique de Louvain, Centre for Molecular Imaging, Radiotherapy and Oncology, B-1200 Brussels, Belgium
[8] Clatterbridge Cancer Centre, Douglas Cyclotron, CH63 4JY Wirral, UK

E-mail: hugo.palmans@npl.co.uk

Abstract
The conversion of absorbed dose-to-graphite in a graphite phantom to absorbed dose-to-water in a water phantom is performed by water to graphite stopping power ratios. If, however, the charged particle fluence is not equal at equivalent depths in graphite and water, a fluence correction factor, k_{fl}, is required as well. This is particularly relevant to the derivation of absorbed dose-to-water, the quantity of interest in radiotherapy, from a measurement of absorbed dose-to-graphite obtained with a graphite calorimeter. In this work, fluence correction factors for the conversion from dose-to-graphite in a graphite phantom to dose-to-water in a water phantom for 60 MeV mono-energetic protons were calculated using an analytical model and five different Monte Carlo codes (Geant4, FLUKA, MCNPX, SHIELD-HIT and McPTRAN.MEDIA). In general the fluence correction factors are found to be close to unity and the analytical and Monte Carlo codes give consistent values when considering the differences in secondary particle transport. When considering only protons

the fluence correction factors are unity at the surface and increase with depth by 0.5% to 1.5% depending on the code. When the fluence of all charged particles is considered, the fluence correction factor is about 0.5% lower than unity at shallow depths predominantly due to the contributions from alpha particles and increases to values above unity near the Bragg peak. Fluence correction factors directly derived from the fluence distributions differential in energy at equivalent depths in water and graphite can be described by $k_{fl} = 0.9964 + 0.0024 \cdot z_{w\text{-eq}}$ with a relative standard uncertainty of 0.2%. Fluence correction factors derived from a ratio of calculated doses at equivalent depths in water and graphite can be described by $k_{fl} = 0.9947 + 0.0024 \cdot z_{w\text{-eq}}$ with a relative standard uncertainty of 0.3%. These results are of direct relevance to graphite calorimetry in low-energy protons but given that the fluence correction factor is almost solely influenced by non-elastic nuclear interactions the results are also relevant for plastic phantoms that consist of carbon, oxygen and hydrogen atoms as well as for soft tissues.

(Some figures may appear in colour only in the online journal)

1. Introduction

The determination of absorbed dose-to-water in reference conditions for clinical proton beams (i.e. beam calibration) is mostly based on standards of absorbed dose-to-water (Andreo *et al* 2000, ICRU 2007), similar to that for radiotherapy external photon and electron beams, where ^{60}Co is often the reference quality. At present, no primary standards for absorbed dose-to-water in proton beams exist and given the increased interest in proton therapy as a clinical viable modality and the growing number of patients treated with it, the development of primary standards is a very actual issue. The successful use of water calorimeters to measure absorbed dose-to-water directly in clinical proton beams has been demonstrated multiple times (Schulz *et al* 1992, Siebers *et al* 1995, Palmans *et al* 1996, Jones *et al* 1999, Medin *et al* 2006, Gagnebin *et al* 2010, Medin 2010 and Sarfehnia *et al* 2010) and dedicated water calorimeters to serve potentially as primary standards for proton beam dosimetry are under development at the Physikalisch-Technische Bundesanstalt (PTB) (Krauss 2007) and the Swiss Federal Office of Metrology (METAS) (Sassowsky and Pedroni 2005). In line with the idea that a network of primary standards is more robust when different metrological methods are available to establish the quantity of absorbed dose-to-water (Andreo *et al* 2000), graphite calorimeters have been developed as well for protons (Palmans *et al* 2004) and carbon ions (Sakama *et al* 2009). Based on the earlier demonstration of a prototype proton calorimeter (Palmans *et al* 2004) the NPL has built a primary standard level graphite calorimeter for proton dosimetry (Palmans *et al* 2007). Other reasons why NPL has chosen to develop a graphite calorimeter are:

(a) NPL's long term expertise with graphite calorimeters (DuSautoy 1996, McEwen *et al* 1998, McEwen and Duane 2000, Duane *et al* 2012, Sander *et al* 2012),

(b) the higher sensitivity of graphite calorimetry as compared to water calorimetry due to the six-fold lower specific heat capacity of graphite,

(c) the possibility of using the isothermal mode of operation which allows much faster repetitive sampling and which is of great advantage when considerable dose gradients are

present close to the point of measurement (as for example the distal edge of a spread out Bragg peak).

Palmans *et al* (2004) singled out the conversion of dose-to-graphite to dose-to-water as the largest contribution to the uncertainty of the absorbed dose-to-water obtained from graphite calorimetry and this has been discussed in more detail by Palmans *et al* (2009) and Karger *et al* (2010). This conversion requires accurate values of the water to graphite mass collision stopping power ratios and fluence correction factors. The interest of this conversion procedure is not limited to graphite calorimetry. Concerning atomic composition (apart from the hydrogen content), most plastic phantoms, tissues and tissue substitutes are characterized by oxygen atoms being totally or partially replaced with carbon atoms. Examples of the former case are polystyrene and polyethylene and of the latter PMMA. While the conversion procedure has been well studied for high-energy photon beams (Burns 1994) and electron beams (McEwen *et al* 1998) this has not been investigated before for proton beams and only a preliminary study has been reported (Palmans *et al* 2011) for protons and a study using a single Monte Carlo code for a number of ion types (Lühr *et al* 2011a). An experimental investigation for the 60 MeV proton beam at the Clatterbridge Cancer Centre (CCC) will be reported in another paper (Palmans *et al* 2013).

Although the influence of secondary charged particles from non-elastic nuclear interactions on the stopping powers, and thus dose, for low-Z media and tissues is considerable (Laitano and Rosetti 2000, Paganetti 2002), the influence on stopping power ratios is considered to be small as for example shown by Medin and Andreo (1997) and Lühr *et al* (2011a) for water-to-air stopping power ratios used in ionization chamber dosimetry. Palmans and Verhaegen (1997) performed Monte Carlo simulations in various low-Z materials and came to the conclusion that the main source of differences in the shape of depth dose curves was due to the differences in the (theoretical) non-elastic nuclear interaction cross sections used in the simulations. The need for fluence correction factors when converting dose distributions from a non-water material to water was demonstrated experimentally and by Monte Carlo simulations for PMMA and polystyrene by Palmans *et al* (2002), for A150, aluminium and copper by Al-Sulaiti *et al* (2010), for water-equivalent plastics by Al-Sulaiti *et al* (2012) and for tissues using Monte Carlo simulations by Palmans and Verhaegen (2005) and Paganetti (2009). Schneider *et al* (2002) performed fluence and dose measurements for 177 MeV protons in a few low-Z materials (PMMA, polyethylene, Teflon and aluminium) compared to water demonstrating good agreement between the two experimental methods. Fluence corrections for PMMA derived from this work would amount to about 1.5% at a water equivalent depth of around 10 cm.

In this work, formal expressions for the definition and calculation of fluence correction factors are given and fluence correction factors for 60 MeV protons have been calculated using an analytical approach and five different Monte Carlo codes.

2. Materials and methods

2.1. Formalism for the fluence correction factor

With a graphite calorimeter, absorbed dose-to-graphite is measured directly in graphite at a depth, z_g: $D_g(z_g)$. The quantity of interest is dose-to-water in a water phantom at the reference depth, z_w: $D_w(z_w)$.

Equivalent depths in water and graphite can be related by the continuous slowing down approximation (csda) ranges, $r_{0,w}$ and $r_{0,g}$, in water and graphite, respectively, and we can assume that for a non-modulated proton beam the depth distal to the dose maximum where

the dose reduces to 80% of the maximum dose is a good estimate of the csda range (Moyers *et al* 2007). In practice it is not always possible to measure at a depth in graphite of which the water equivalent depth, $z_{w\text{-eq}}$, coincides exactly with z_w. Hence the water equivalent depth of the measurement depth in graphite is obtained as:

$$z_{w\text{-eq}} = z_g \cdot \frac{r_{0,w}}{r_{0,g}}. \tag{1}$$

Throughout this paper z_w, $z_{w\text{-eq}}$, z_g, $r_{0,w}$ and $r_{0,g}$ will always be expressed in terms of the mass thickness in g cm^{-2}.

The ratio of dose-to-water in the water phantom and dose-to-graphite in the graphite phantom can be derived from the charged particle fluence differential in energy, for all charged particle types i, at the equivalent depths in both phantom materials:

$$\frac{D_w(z_{w\text{-eq}})}{D_g(z_g)} = \frac{\sum_i \left[\int_0^{E_{\max,i}} \Phi_{E,w,i}(E) \cdot \left(\frac{S_{el,i}(E)}{\rho} \right)_w \cdot dE \right]}{\sum_i \left[\int_0^{E_{\max,i}} \Phi_{E,g,i}(E) \cdot \left(\frac{S_{el,i}(E)}{\rho} \right)_g \cdot dE \right]} \tag{2}$$

where $S_{el,i}/\rho$ is the electronic mass collision stopping power and $E_{\max,i}$ the maximum energy of particle type i in the fluence distribution. This equation is exact when all charged particles are considered (i.e. also those produced by neutron interactions) and the fluence distributions are obtained by tracking all charged particles down to zero kinetic energy.

If the charged particle fluence distributions in both phantom materials are equal, i.e. $\Phi_{E,w,i} = \Phi_{E,g,i}$, for all energies and all charged particle types, i, then $D_g(z_g)$ and $D_w(z_w)$ are related by the water-to-air mass electron collision stopping power ratio for the total charged particle fluence distribution in graphite: $s_{w,g}(\Phi_g)$.

$$D_w(z_{w\text{-eq}}) = D_g(z_g) \cdot s_{w,g}(\Phi_g) \tag{3}$$

where

$$s_{w,g}(\Phi_g) = \frac{\sum_i \left[\int_0^{E_{\max,i}} \Phi_{E,g,i}(E) \cdot \left(\frac{S_{el,i}(E)}{\rho} \right)_w \cdot dE \right]}{\sum_i \left[\int_0^{E_{\max,i}} \Phi_{E,g,i}(E) \cdot \left(\frac{S_{el,i}(E)}{\rho} \right)_g \cdot dE \right]}. \tag{4}$$

The stopping power ratio could be equally calculated from the charged particle fluence in water.

When the fluence distributions are not equal in both phantoms the same relation can be used but with addition of a correction factor that accounts for the difference in fluence:

$$D_w(z_{w\text{-eq}}) = D_g(z_g) \cdot s_{w,g}(\Phi_g) \cdot k_{fl} \tag{5}$$

From equations (2), (4) and (5) it is clear that the fluence correction factor k_{fl} according to this definition is given by:

$$k_{fl} = \frac{\sum_i \left[\int_0^{E_{\max,i}} \Phi_{E,w,i}(E) \cdot \left(\frac{S_{el,i}(E)}{\rho} \right)_w \cdot dE \right]}{\sum_i \left[\int_0^{E_{\max,i}} \Phi_{E,g,i}(E) \cdot \left(\frac{S_{el,i}(E)}{\rho} \right)_w \cdot dE \right]}. \tag{6}$$

This factor could be interpreted as the conversion of dose-to-water in the graphite phantom, to dose-to-water at an equivalent depth in the water phantom.

Note that in equation (4) the fluence is the same in numerator and denominator and only the interaction data are different, while in equation (6) the interaction data are the same but the fluence distributions are different. Equation (5) could thus be regarded as splitting the conversion into an interaction data related part and a part related to the difference in fluence.

Of course the effects of fluence and interaction data are intermixed and we could as well propose:

$$D_w(z_{w\text{-eq}}) = D_g(z_g) \cdot s_{w,g}(\Phi_w) \cdot k'_{fl} \tag{7}$$

where

$$s_{w,g}(\Phi_w) = \frac{\sum_i \left[\int_0^{E_{\max,i}} \Phi_{E,w,i}(E) \cdot \left(\frac{S_{\mathrm{el},i}(E)}{\rho} \right)_w \cdot \mathrm{d}E \right]}{\sum_i \left[\int_0^{E_{\max,i}} \Phi_{E,w,i}(E) \cdot \left(\frac{S_{\mathrm{el},i}(E)}{\rho} \right)_g \cdot \mathrm{d}E \right]} \tag{8}$$

and

$$k'_{\mathrm{fl}} = \frac{\sum_i \left[\int_0^{E_{\max,i}} \Phi_{E,w,i}(E) \cdot \left(\frac{S_{\mathrm{el},i}(E)}{\rho} \right)_g \cdot \mathrm{d}E \right]}{\sum_i \left[\int_0^{E_{\max,i}} \Phi_{E,g,i}(E) \cdot \left(\frac{S_{\mathrm{el},i}(E)}{\rho} \right)_g \cdot \mathrm{d}E \right]}. \tag{9}$$

The steps can be interpreted as a conversion from dose-to-graphite in graphite to dose-to-graphite in water by the fluence correction factor and then a conversion from the latter to dose-to-water in water.

It is interesting to think what the meaning of the ratio $k_{\mathrm{fl}}/k'_{\mathrm{fl}}$ is. If both were pure fluence correction factors then this ratio should be unity. However, the stopping powers and fluence are entangled by the convolutions in the above equations so they cannot be entirely separated. From equations (5) and (7) it is clear that the ratio $k_{\mathrm{fl}}/k'_{\mathrm{fl}}$ is the ratio of water-to-graphite electronic mass stopping power ratios for the spectra in water and graphite. The deviation from unity thus reflects in some way how much influence of the stopping power energy dependence is on what we have called the fluence correction factor. Again, if the shape of the spectra would be exactly the same for all charged particle types and the amplitude of the fluence distributions for all particles have the same ratio (between water and graphite) then the ratio $k_{\mathrm{fl}}/k'_{\mathrm{fl}}$ would become unity and again both k_{fl} and k'_{fl} could be considered as pure fluence correction factors.

The steps according to equations (4), (5) and (6) are more logical in converting dose-to-graphite measured in graphite using graphite calorimetry to dose-to-water in a water phantom.

These equations formalize the two ways we have used to calculate the fluence correction factor using Monte Carlo methods:

(i) k_{fl} calculated directly using equation (6) by Monte Carlo simulation of the fluence distributions differential in energy for all charged particle types in both phantoms to calculate the dose integrals. Some simplifications may be justified but those should all be tested. The contribution of secondary particles other than protons to the dose is small and may be negligible in the ratio. If this is the case and in addition the proton spectra are equal but merely the number of protons are different, then a simple calculation of the number of protons may be sufficient to determine the ratio. There are some indications that this could work reasonably well in a low energy beam; the relative contribution of secondary protons to the dose is only a few percent and the proton scatter is small so that the number of protons (corresponding to planar fluence) is a reasonable estimate of the fluence. Nevertheless it may be too simplistic to model the small corrections we are looking for.

(ii) k_{fl} calculated using equation (5) by scoring absorbed doses $D_w^{\mathrm{MC}}(z_{w\text{-eq}})$ and $D_g^{\mathrm{MC}}(z_g)$ at equivalent depths in water and graphite, respectively, within the Monte Carlo simulation and the stopping power ratio using equation (4):

$$k_{\mathrm{fl}} = \frac{D_w^{\mathrm{MC}}(z_{w\text{-eq}})}{D_g^{\mathrm{MC}}(z_g) \cdot s_{w,g}(\Phi_g^{\mathrm{MC}})}. \tag{10}$$

At first sight, it may seem as if there is not much advantage compared to the first method since one still has to calculate the fluence distribution in one of the simulations (and if it can be done for one material it can be done as well for the other). But here simplifications may work better since we have to deal only with a stopping power ratio for one and the same

spectrum. Medin and Andreo (1997) showed that the contribution from secondary protons to these stopping power ratios results in differences smaller than 0.1%. Contributions from heavier secondary particles are likely smaller. So, if only the primary proton peak is important, and given that the distribution of these primary protons is narrow for most depths, stopping power ratios for mono-energetic protons will probably be accurate enough as long as it is not too close to the Bragg peak and we could rely on the peak energy as a function of depth or the residual range to estimate an accurate value of the water-to-graphite stopping power ratio.

It is also clear that both methods (without any of the suggested simplifications) are actually strongly linked. The only difference is that in the second method two doses are calculated during the simulation whereas in the first method doses are calculated retrospectively from the fluence distributions. So the results should be equal if the scoring of dose and fluence in the code is consistent.

All the quantities can be calculated in one run per material. Ideally the cavity integrals are all calculated within the Monte Carlo simulation avoiding problems with the resolution of binning but probably it is accurate enough to calculate the integrals afterwards from the calculated fluence distributions. Track ends of particles falling below the Monte Carlo energy cut-offs need to be accounted in the dose deposition but probably not for the stopping power ratios.

2.2. Analytical simulation

An analytical approach to estimate the removal of primary protons from the beam has been described in detail in another publication (Al-Sulaiti *et al* 2010) and is extended here to include energy depositions due to secondary particles emerging from non-elastic nuclear interactions. The following simplifications are made:

- primary protons are tracked along a straight line, without considering scattering and energy straggling and their energy loss is calculated in the csda,
- the energy given to any secondary charged particle emerging from a nuclear interaction is deposited on the spot,
- the energy transferred to neutrons and gamma rays does not contribute to dose.

This is of course overly naïve and in particular it can be expected that secondary charged particles can travel a considerable distance away from the point where they are generated. Nevertheless, the second simplification may be a reasonable approximation if secondary charged particle equilibrium is established and, as we will see, the results of the analytical approach can provide insight into the source of fluence correction factors.

In brief, along a grid of predefined step lengths, the average energy loss of primary protons is derived using the stopping powers from ICRU Report 49 (ICRU 1993) to obtain the primary proton energy $E_{p_{\text{prim}}}$ at the back of each slab. The attenuation of primary particles due to non-elastic nuclear interactions over each step is calculated using the total non-elastic nuclear interaction cross sections from ICRU Report 63 (ICRU 2000) providing estimates of the primary proton fluences in water and graphite as a function of depth, $\Phi_w^{p_{\text{prim}}}(z_{w\text{-eq}})$ and $\Phi_g^{p_{\text{prim}}}(z_g)$, per unit of incident fluence. Dose-to-water in water phantom is then calculated as

$$D_w(z_{w\text{-eq}}) = \Phi_w^{p_{\text{prim}}}(z_{w\text{-eq}}) \cdot \left(\frac{S_{\text{el},p}(E_{p_{\text{prim}}})}{\rho} \right)_w + \Phi_w^{p_{\text{prim}}}(z_{w\text{-eq}}) \cdot \frac{N_A}{A^w} \cdot \sum_i \sigma_{\text{prod},i}^O \cdot \left\langle W_{\text{rec},i}^O \right\rangle \quad (11)$$

Where N_A is Avogadro's number, A^w is the molecular weight of water and $\sigma_{\text{prod},i}^O$ and $\left\langle W_{\text{rec},i}^O \right\rangle$ are the production cross section and the mean energy of the recoil spectrum, respectively, of

charged particle type i resulting from nonelastic nuclear interactions of a proton projectile with energy $E_{p_{\text{prim}}}$ and an oxygen atom as target nucleus.

Similarly

$$D_g(z_g) = \Phi_g^{p_{\text{prim}}}(z_g) \cdot \left(\frac{S_{\text{el},p}\left(E_{p_{\text{prim}}}\right)}{\rho}\right)_g + \Phi_g^{p_{\text{prim}}}(z_g) \cdot \frac{N_A}{A^C} \cdot \sum_i \sigma_{\text{prod},i}^C \cdot \left\langle W_{\text{rec},i}^C \right\rangle \tag{12}$$

where A^C is the atomic weight of a carbon atom and $\sigma_{\text{prod},i}^C$ and $\left\langle W_{\text{rec},i}^C \right\rangle$ are the production cross section and the mean energy of the recoil spectrum, respectively, of charged particle type i resulting from nonelastic nuclear interactions of a proton projectile with energy $E_{p_{\text{prim}}}$ and a carbon atom as target nucleus.

The fluence correction factor is then obtained in a similar way as with equation (10):

$$k_{\text{fl}} = \frac{D_w(z_{w\text{-eq}})}{D_g(z_g) \cdot \left(\frac{S_{\text{el},p}\left(E_{p_{\text{prim}}}\right)}{\rho}\right)_w \Big/ \left(\frac{S_{\text{el},p}\left(E_{p_{\text{prim}}}\right)}{\rho}\right)_g} \tag{13}$$

where the stopping power ratio is calculated for mono-energetic protons with energy $E_{p_{\text{prim}}}$. The validity of using this mono-energetic stopping power ratio is difficult to verify with the analytical approach since for a full stopping power ratio (including all charged particles) slowing down spectra need to be calculated for all secondary charged particles. Lühr *et al* (2011a, 2011b) showed that this is usually a good approximation at depths shallower than the Bragg peak region especially for ions heavier than protons and the validity of this approximation will be further verified here using the Monte Carlo simulations.

2.3. Monte Carlo simulation

Depth dose curves and fluence distributions differential in energy were simulated for a 60 MeV mono-energetic proton pencil beam incident on slab phantoms of graphite ($\rho = 1.78$ g cm^{-3}) and water ($\rho = 1.0$ g cm^{-3}) using five different Monte Carlo codes or code systems: McPTRAN.MEDIA (Palmans 2005), Geant4 (Agostinelli *et al* 2003), FLUKA (Ferrari *et al* 2005, Battistoni *et al* 2007), SHIELD-HIT (Dementyev and Sobolevsky 1999, Gudowska *et al* 2004) and MCNPX (Pelowitz 2005).

McPTRAN.MEDIA simulations were performed for 60 MeV mono-energetic protons. McPTRAN.MEDIA is an extension of PTRAN (Berger 1993) allowing transport in different media than water using stopping powers from ICRU Report 49 and total non-elastic nuclear interaction cross sections from ICRU Report 63 (Palmans 2005). Since this code does not transport secondary particles resulting from non-elastic nuclear interactions these simulations are merely for illustrative purposes and to enable a comparison with the analytical results.

Geant4 simulations were performed for mono-energetic 60 MeV pencil beams of protons using version 4.9.0 of the Geant4 toolkit (Agostinelli *et al* 2003). The simulations were based on the hadrontherapy advanced example using the Precompound model for non-elastic nuclear interactions and 3×10^7 proton histories were simulated for each material. Simulations of 10^6 histories were also performed using three models for non-elastic nuclear interactions: Precompound, Bertini intranuclear cascade (QGSP+BERT) and binary intranuclear cascade (QGSP+BIC). For electromagnetic interactions, low-energy models were used for all particles using the default ICRU Report 49 stopping power parameterization. Production cut-offs for photons, electrons and positrons were set to a range of 0.005 mm. The phantom was a 100 mm diameter cylinder and slab thicknesses were 0.05 mm for graphite and 0.07 mm for water.

FLUKA simulations were performed using version 2008.3c in a cylindrical phantom of radius 50 mm and a thickness of 32 mm and the total energy deposited in 0.1 mm thick slabs

was determined using the USRBIN scoring option. 10^6 proton histories were simulated for each material. Physics settings suitable for hadrontherapy calculations (DEFAULTS card set to HADROTHE) were used together with new hadronic evaporation models and inclusion of heavy ion nuclear interactions. The particle transport threshold was 100 keV except for neutrons which were transported down to thermal energies.

SHIELD-HIT simulations were performed using two versions. Version 08 was used to simulate 10^6 protons of 60 MeV and their nuclear fragments down to 25 keV in water and graphite cylindrical phantoms of 200 mm diameter and 40 mm height, divided into slabs 0.1 mm thick. An improved track-length fluence estimator was used to determine fluence differential in energy for all particles in both media, which subsequently was refined and implemented in Version 10A. Water stopping powers were those from the errata to ICRU Report 73 (ICRU 2005, Sigmund *et al* 2009), based on a value of the mean excitation energy, *I*, of 78.0 eV, and the transport included Vavilov-Landau energy straggling and Molière multiple scattering. Version 10A (Hansen *et al* 2012) was used to simulate $5 \ 10^7$ initial protons and their nuclear fragments. A major improvement with respect to this study is the online scoring of the cavity integrals used to calculate the fluence correction factor with equation (6). It is done during the calculation without the need of post processing (except for calculating the ratio of the two integrals) as described earlier (Lühr *et al* 2011a). One solid cylinder was used as target instead of slabs with a thickness of 0.1 mm. Three different stopping power data for water were applied using the Bethe formula with the *I*-values 75 and 78 eV (Lühr *et al* 2012) and the tabulated ICRU data (ICRU 1993).

MCNPX simulations were performed using version 2.4.0 for mono-energetic 60 MeV protons on a cylindrical slab phantom with slabs of 1 mm thickness and a radius of 40 mm. 10^7 proton histories were simulated. The nuclear cross section data used were from the LA150H library. The physics model parameters for particle transport were as follows: maximum energy of 100 MeV, default cut-off energy of 1 MeV for protons and 4 MeV for alpha particles, charged particle straggling and stop light ion recoil (default parameter). Tally 1 (F1: fluence integrated over cell surface) and tally 6 (F6: energy deposition average over the cell) were used to score protons and alpha particle fluences and energy loss, respectively, as a function of depth.

3. Results and discussion

3.1. Analytical simulations

Figure 1 shows the results of the analytical simulations taking into account the contributions from different subsets of secondary charged particle types. The curve for primary protons only is the result of the difference in removal of primary protons from the beam by non-elastic nuclear interactions and is consistent with earlier calculations presented by Palmans *et al* (2009). Since the primary proton fluence at the surface is the same in both phantoms, k_{fl} considering only primary protons is unity at the surface. This is not the case when also secondary protons are included and the deviation from unity becomes larger at the surface when gradually including other charged particle types. This illustrates the relative importance of contributions from different secondary charged particle types according the interaction cross sections from ICRU Report 63. At larger depths all the curves converge to the value for primary protons only since the contributions of secondary particles becomes negligible (no nuclear interactions take place at those depths).

It has been suggested by Palmans *et al* (2002, 2009) that converting the contributions from the electromagnetic interactions (characterized by the electronic stopping powers) and
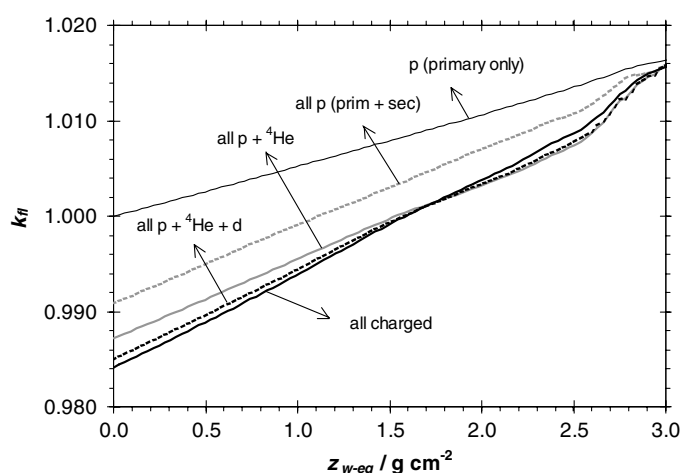
Figure 1. Analytically calculated fluence correction factors according to equations (11–13) for the conversion of dose-to-graphite in a graphite phantom to dose-to-water in a water phantom at an equivalent depth in a 60 MeV mono-energetic proton beam. The different curves are considering different subsets of secondary charged particle types as indicated in the graph (p = protons, d = deuterons).

the contributions from the secondary particles separately by the appropriate interaction and production cross sections in the conversion procedure, the fluence correction factor (which is then different from the one defined here) could become unity at the surface for all particles and would be quite similar as for the primary protons only. This proposed procedure is only applicable if all energy of secondary particles is deposited on the spot and would thus be valid for this analytical approach. However, since this represents an unrealistic assumption and in addition since it is in practical situations often not possible to know how to split the different contributions, this idea is not further pursued here.

It can be assumed that in reality the transport of secondary particles along the beam direction, which has not been taken into account in the analytical model, will result in a fluence correction factor which is closer to the one for primary protons only (and thus closer to unity) at the surface while at larger depths where charged particle equilibrium is established (even if it is only a transient equilibrium) the values in figure 1 will be closer to reality. Furthermore, at larger depths the momentum transfer to the secondary particles becomes smaller and the assumption of a deposition on the spot becomes better. It is also clear from figure 1 that the main contributions are protons (primary and secondary) and alpha particles.

3.2. Monte Carlo simulations

Figure 2 shows the results obtained from McPTRAN.MEDIA compared with the analytical curves from figure 1 for primary protons only and for all charged particles. Calculating simply the ratio of the number of primary protons as a function of depth the agreement with the analytical calculation for primary protons only is perfect. Since McPTRAN.MEDIA only calculates the spectra of primary protons the fluence correction factors obtained with equation (6) can also be compared with the same analytical curve. The agreement is also good except that at larger depths in the vicinity of the Bragg peak a small deviation is visible. This is likely related to the widening energy spectrum due to energy straggling and possibly a
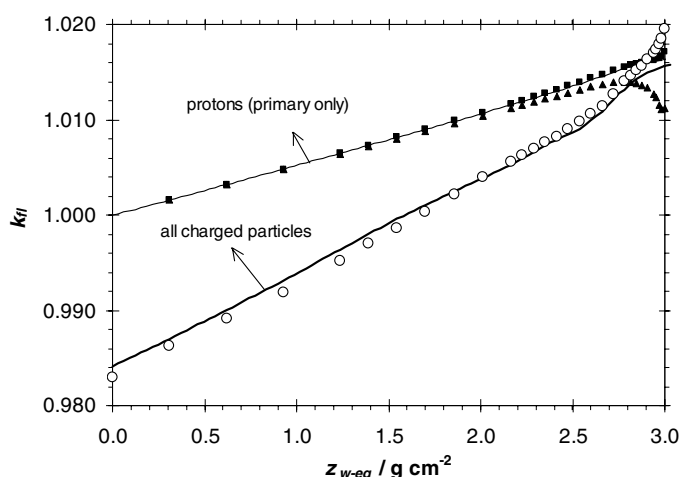
Figure 2. Fluence correction factors for a 60 MeV mono-energetic proton beam calculated with McPTRAN.MEDIA using equation (6) applied to the primary proton spectrum (triangles), as a ratio of number of primary protons (squares) or using equation (10) applied to all energy depositions by charged particles and using the proton spectrum for the stopping power ratio (hollow circles). The lines are two of the curves from figure 1 as indicated.

smaller influence of differences in scattering. k'_{fl} according to equation (9) was also calculated but was found to be no more than 0.002% different from k_{fl} for any depth until the Bragg peak. When the fluence correction factor is calculated according to equation (10), including the locally deposited secondary charge particle contributions, again an excellent agreement with the corresponding analytical curve was found except for an increasing deviation at larger depths. Since the stopping powers and nuclear interaction data used in McPTRAN.MEDIA and the analytical model are the same, the good agreement for both methods shows that scattering and straggling have a very minor influence on the results except in the vicinity of the Bragg peak where absolute dose measurements would normally not be made (the issue of fluence correction factors in spread-out Bragg peaks, where obviously the Bragg peak contributes to the dose at the point of measurement, will be addressed in a follow-on paper, Palmans *et al* 2013).

Figure 3 shows results from the Geant4 simulations. The type-A uncertainties until a depth of about 2.9 g cm^{-2} are smaller than 0.03%. The observations in figure 3 are consistent with the analytical simulations keeping in mind the suggestion that close to the surface, k_{fl} should be closer to unity while at larger depths they become closer to the analytical result. When considering only protons, k_{fl} is unity at the surface indicating that any energy transfers to secondary protons are transported to larger depths. This is consistent with a secondary proton fluence build up effect. When the contributions from deuterons, tritium and alpha particles are considered as well, the k_{fl} values are lower by about 0.5% at the surface and by lesser amounts at larger depths. The step feature around the middle of the range remains unexplained but is related to the contribution of alpha particles and probably due to the nuclear models or nuclear data used for this particle type. Similar features related to the contribution of alpha particles were observed in an 80 MeV per nucleon carbon ion beam (Rossomme *et al* 2013). The difference between k_{fl} and k'_{fl} is negligible (smaller than 0.002%) for all calculations. This confirms largely the independence of the stopping power ratio and the fluence correction factor.
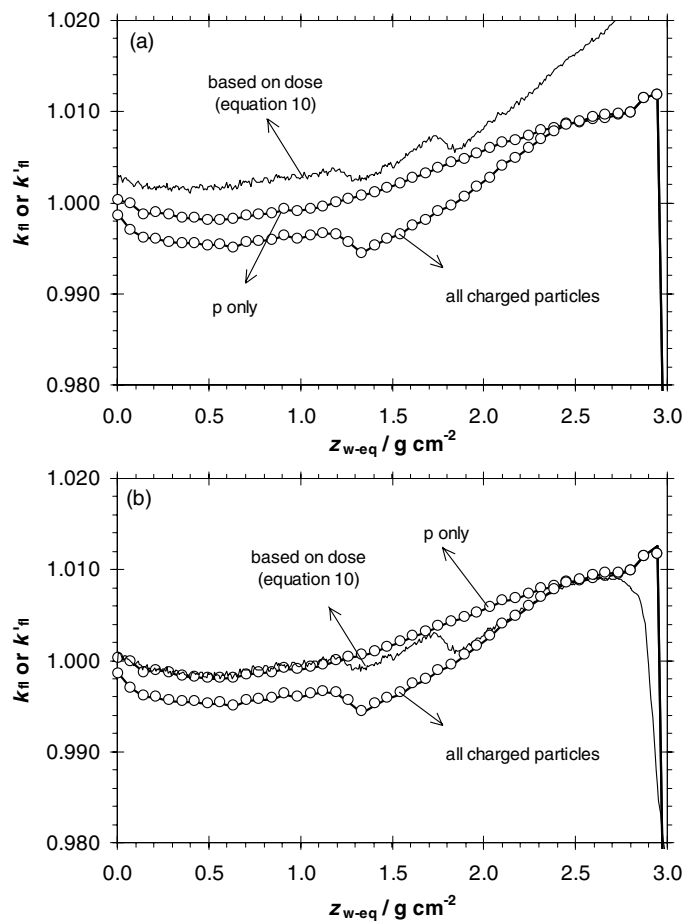
Figure 3. Fluence correction factors for 60 MeV mono-energetic protons calculated using Geant4 with the Precompound nuclear models. The thick lines are k_{fl} values obtained from equation (6) using either the proton spectrum only or all the charged particle spectra as indicated in the graph. The symbols, almost coinciding with the thick lines are corresponding k'_{fl} values obtained from equation (9). The thin lines are obtained from the calculated depth dose distributions using equation (10). In figure (a) stopping powers from ICRU Report 49 were used for the calculation of the cavity integrals in equations (6), (9) and (8) while in figure (b) the stopping powers effectively used in the transport simulations were used for the calculation of the cavity integrals (see the explanation in the text).

The values about 0.5% lower than unity can be attributed entirely to the contribution of alpha particles. Indeed, the production cross section of alpha particles per unit of atomic weight of the target atom for protons incident on carbon is larger than for protons incident on oxygen as target atom (a factor 1.7 at 60 MeV increasing to a factor 10 at 11 MeV). On the other hand the mean energy of alpha particles resulting from carbon as target atom is lower than for oxygen as target atom. The product of the number of alpha particles and their mean energy results in a ratio of the amount of energy transferred to alpha particles of 1.4 at 60 MeV to 2.6 at 17 MeV. Given the contribution from alpha particles to dose of about 0.5% in water, this would explain the magnitude of the effect when comparing graphite and water as target media. The contribution of other charged particles was found to be negligible
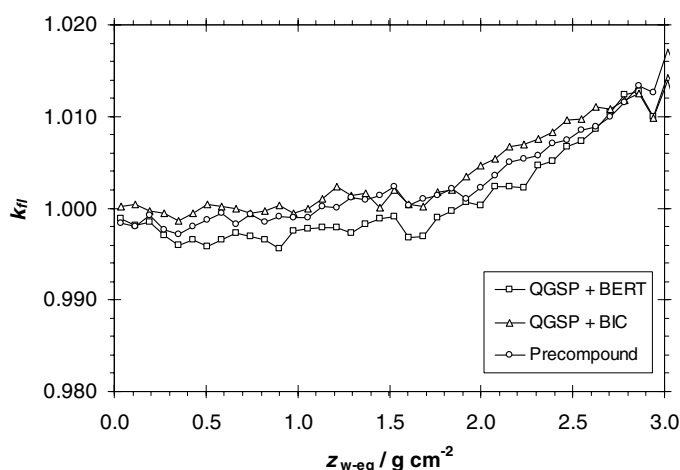
Figure 4. Fluence correction factors for 60 MeV mono-energetic protons calculated with Geant4 from calculated depth dose distributions using equation (10) and the stopping powers effectively used in the simulations. The three data sets correspond to simulations using three different nuclear interaction models as indicated in the legend.

which is reasonably consistent with the analytical predictions, although a small effect from mainly deuterons is seen in the analytical results of figure 1. In terms of the contribution to the total dose the contribution of deuterons is much smaller than in the analytical calculations (this is consistent with the small contributions reported by Paganetti 2002), which indicates a discrepancy between the data resulting from the nuclear models in Geant4 and the ICRU Report 63 tables.

In the Geant4 simulations the ICRU Report 49 stopping power parameterization was used in the physics list. Hence, in a first analysis, shown in figure 3(a), ICRU Report 49 stopping powers were used for the calculation of the cavity integrals in the evaluations of fluence correction factors using equations (6) and (9) and for the stopping power ratio in equation (8). However, dumping stopping power tables during the Geant4 simulations revealed that the ones actually used in the transport simulations (determining also the energy loss calculated over transport steps) are substantially different from ICRU Report 49 tables over certain energy ranges, which explains the inconsistent results based on both methods seen in figure 3(a). This inconsistency largely disappears when using stopping powers that are more representative of those used in the simulations for the calculation of the cavity integrals as done in figure 3(b). Note that this discrepancy is entirely due to the difference in the values obtained with equation (10) while the values obtained with equations (6) and (9) do not significantly depend on which stopping powers are used in the cavity integrals (this can be understood by the fact that the same stopping power data are used in the numerator and the denominator in the latter expressions). Note also that the Geant4 data in Palmans *et al* (2011) were also calculated using equation (10) with stopping powers in equation (8) from ICRU Report 49 stopping power data leading to the k_{fl} values of larger than 1.020 at depths near the Bragg peak.

The results based on equation (6) are almost not influenced by the stopping power set used, which can be explained by the fact that stopping powers for only one material are used but it also illustrates the independence of the fluence correction factor from the stopping power ratio. This also minimizes the question of whether or not one has to use the stopping powers for graphite or amorphous carbon in the calculation of these cavity integrals (in all the simulations
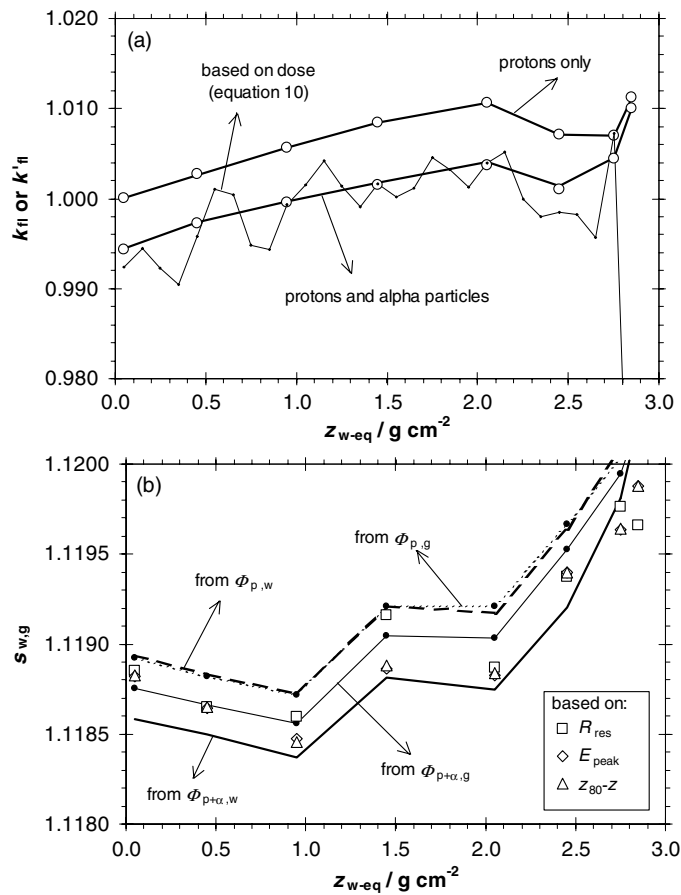
Figure 5. (a) Fluence correction factors for 60 MeV mono-energetic protons calculated using FLUKA. The thick lines are k_{fl} values obtained from equation (6) using either the proton spectrum only or all the charged particle spectra as indicated in the graph. The symbols, almost coinciding with the thick lines are corresponding k'_{fl} values obtained from equation (9). The thin line is obtained from the calculated depth dose distributions using equation (10). (b) Water-to-graphite stopping powers derived in various ways as explained in the text.

in this work, except those with SHIELD-HIT, those for graphite have been used). It was also found that calculating the stopping power ratio in various ways (considering all heavy charged particles, considering only protons or considering simply mono-energetic protons based on the residual range) resulted in negligible differences. A more extensive example of that will be shown for the FLUKA simulations below.

Figure 4 shows results obtained with three different nuclear interaction models as described in section 3.2 demonstrating that different nuclear interaction models in Geant4 give consistent results. The fluctuations in figure 4 reflect the type A uncertainty of 0.2% on the Monte Carlo calculated data points.

Figure 5 shows the results from the FLUKA simulations. Again there is no significant difference between k_{fl} and k'_{fl} values derived using equations (6) and (9) and the results including alpha particles are about 0.5% lower than those considering only protons. No other contributions were found to have a significant influence on the results. The results based on dose
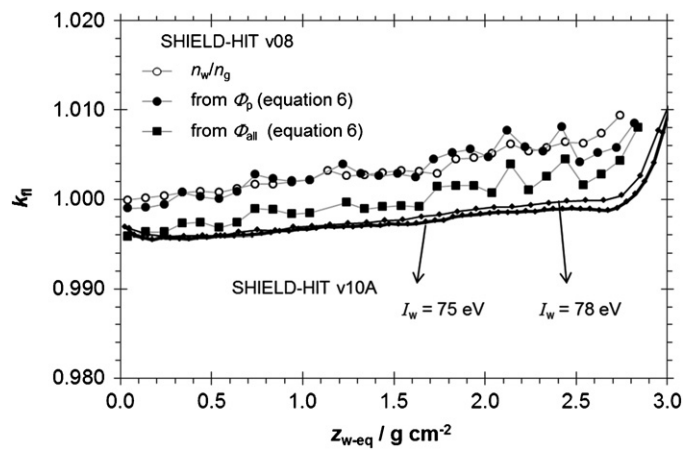
Figure 6. Fluence correction factors for 60 MeV mono-energetic protons calculated with the fluence based approach (equation (6)) using SHIELD-HIT v08 from either the total number of protons at equivalent depths in both phantoms, from the proton fluence distribution differential in energy or from the fluence distribution for all heavy charged particles and using SHIELD-HIT10A for the fluence distribution for all heavy charged particles using two different values of the mean excitation energy I_w for the water stopping powers.
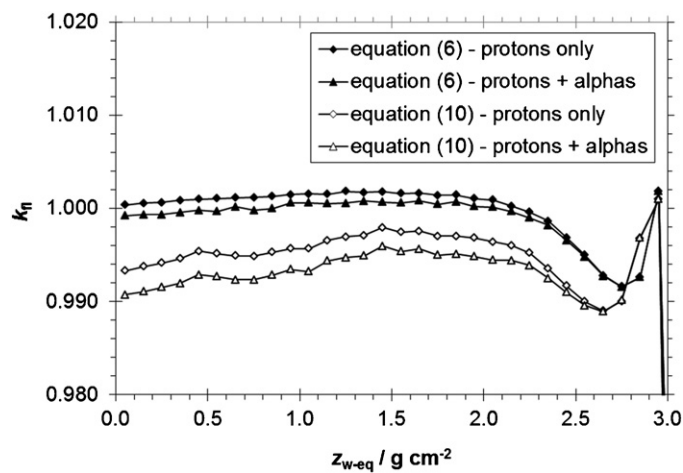

Figure 7. Fluence correction factors for 60 MeV mono-energetic protons calculated with both approaches using MNCPX.

calculations are consistent with those based on the charged particle fluence. The fluctuations on the dose based calculation are consistent with the type A uncertainties of around 0.5%. The difference between using ICRU49 stopping powers and the FLUKA stopping powers used in the simulations was found to be very small (<0.1% over the relevant energy range).

Water to graphite stopping power ratios derived from the FLUKA simulations in various ways are shown in figure 5(b): (i) from the fluence of protons and alpha particles in water (data points connected by thick continuous line), (ii) from the fluence of protons and alpha particles in graphite (data points connected by thin continuous line), (iii) from the fluence of
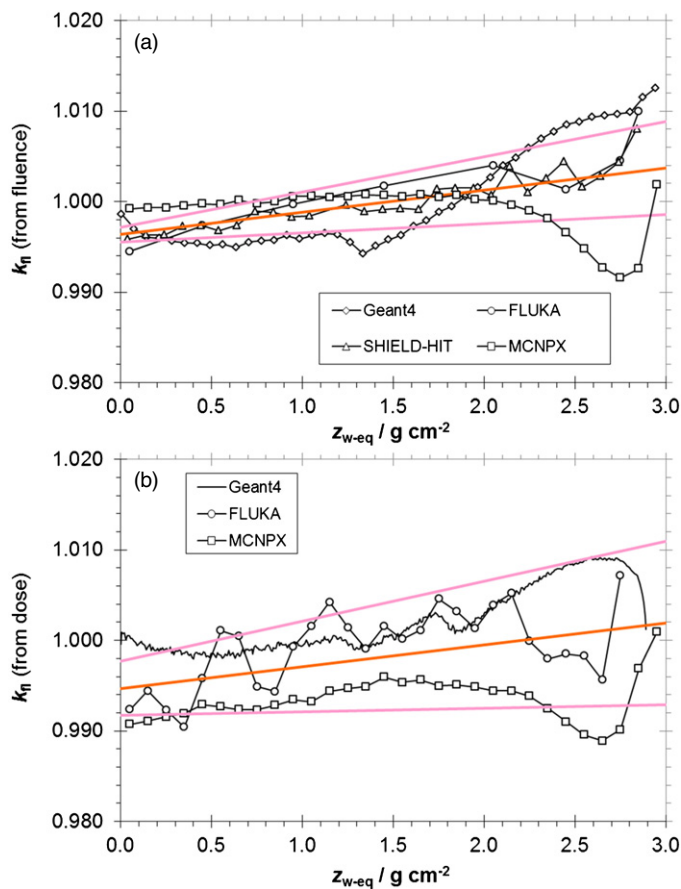
Figure 8. Results from four codes for k_{fl} (a) from equation (6) and from three codes (b) from equation (10) for 60 MeV mono-energetic protons. The orange lines (central grey lines in the printed version) are linear fits to the average of the three curves from the surface to a depth of 2.7 g cm^{-2} while the pink lines (upper and lower grey lines in the printed version) represent a 2σ interval of uncertainty estimates based on linear fits to the root mean square deviations from the mean values.

protons only in water (data points connected by thick dashed line), (iv) from the fluence of protons only in graphite (data points connected by thin dashed line), (v) for mono-energetic protons that have the same csda range as the residual range R_{res}, i.e. the distance to the 10% dose level on the distal edge, $z_{10}-z$, (vi) for mono-energetic protons with energy equalling the peak energy, E_{peak}, of the proton fluence distribution differential in energy and (vii) for mono-energetic protons that have the same csda range as the distance to the 80% dose level on the distal edge, $z_{80}-z$. The data in figure 5(b) illustrate that the differences in stopping power ratios are very small and that stopping power ratios for mono-energetic protons are sufficiently accurate in the energy range considered in this study.

Figure 6 shows results obtained using two versions of SHIELD-HIT. Similar observations as for Geant4 and FLUKA can be made. When considering only protons, the results using the entire fluence spectrum are equal to those obtained by simply taking the total number of protons similarly as in the McPTRAN.MEDIA results. When the fluence correction factor is

derived from the entire charged particle spectrum the results are about 0.4% lower, consistent with the other results. The results obtained with version 10A of SHIELD-HIT are reasonably consistent, albeit slightly lower, and indicate again that the influence of the stopping powers themselves on the fluence correction factors is small.

The results from the MCNPX simulations are shown in figure 7. Type-A uncertainties are below 0.03% until the Bragg peak. The influence of alpha particles is again clear from the graph. The substantial difference between the fluence based approach (equation (6)) and the dose based approach (equation (10)) could indicate that there is a discrepancy between the scoring algorithms and the stopping powers used (care was taken that the same stopping powers as used in the simulations were used for the evaluation of equation (8)) or it could be the result of artefacts similar as those shown by Reynaert *et al* (2002). No obvious explanation was found and it goes beyond the scope of this paper to study this in detail within the code.

Figure 8(a) summarizes the results obtained by the fluence based approach (equation (6)) from Geant4, FLUKA, SHIELD-HIT and MCNPX and shows good consistency. The consistency of the three dose based calculations in figure 8(b) is slightly worse, which can be partly attributed to the larger type-A uncertainties of those calculations for the same number of histories but also due to larger discrepancies between the three codes. The overall picture is that at shallow depths k_{fl} is about 0.5% below unity and increases with depth for all codes and both approach a value slightly above unity.

For the fluence based approach the linear fit to the mean values of the four codes, shown in figure 8(a), is given by:

$$k_{\mathrm{fl}} = 0.9964 + 0.0024 \cdot z_{w\text{-eq}} \quad \text{(with } z_{w\text{-eq}} \text{ in g cm}^{-2}\text{)} \tag{14}$$

with a relative standard uncertainty (derived from the average value of the root mean square of the deviations from the linear fit) of 0.2%.

For the dose based approach a similar linear fit to the mean values of the three codes, shown in figure 8(b), is given by:

$$k_{\mathrm{fl}} = 0.9947 + 0.0024 \cdot z_{w\text{-eq}} \quad \text{(with } z_{w\text{-eq}} \text{ in g cm}^{-2}\text{)} \tag{15}$$

with a relative standard uncertainty derived in a similar way of 0.3%. Both results are consistent with each other, within the uncertainties. Given the lower uncertainty of the results leading to equation (14) it is recommended to use that expression.

At a depth of about 1.5 cm which would be suitable for absolute measurements k_{fl} is unity within the uncertainties for all codes and both approaches. That this depth is about half of the range is a coincidence since it is the result of two opposing effects (a different loss of primary protons and a different production of secondary particles and their transport) and is only valid for 60 MeV protons.

4. Conclusions

Fluence correction factors to correct the conversion from dose-to-graphite in a graphite phantom to dose-to-water in a water phantom for 60 MeV protons were obtained using analytical simulations and Monte Carlo simulations using five Monte Carlo codes. These results are of direct relevance to graphite calorimetry in low-energy mono-energetic proton beams such as the ones used in Clatterbridge.

The analytical results show that considering only primary protons the fluence correction factor is unity at the surface and increased with depth showing that more primary protons are removed from the beam in graphite per unit of water equivalent depth as compared to water. When taking into account local dose depositions due to secondary charged particles

emerging from non-elastic nuclear interactions, the fluence correction factors are reduced at shallow depths to values below unity, dominated by the contributions from secondary protons and alpha particles and to a lesser extent by other charged particles.

The results using McPTRAN.MEDIA form a bridge between the analytical results and the other Monte Carlo codes since doses deposited by secondary particles from nuclear interactions are deposited on the spot, like in the analytical simulations, but protons are tracked using realistic scattering and energy straggling models as in the other Monte Carlo codes. The results show that scattering and straggling have almost no influence on the calculated fluence correction factors.

The results obtained with other Monte Carlo codes show that:

- k_{fl} and k'_{fl} are equal within 0.002%,
- k_{fl} at shallow depths is closer to unity than in the analytical and McPTRAN.MEDIA simulations which can be explained by the transport of secondary particles (mainly the secondary protons),
- k_{fl} at shallow depths is about 0.5% below unity mainly due to the contribution of alpha particles,
- the influence of the stopping powers is small when k_{fl} is calculated from its definition using equation (6),
- when k_{fl} is calculated from dose ratios using equation (10) the stopping powers used for the water-to-graphite stopping power ratio in equation (8) should be consistent with those used in the Monte Carlo simulations,
- for the calculation of water to graphite stopping power ratios at equivalent depths and fluence correction factors, stopping power ratios for mono-energetic protons are sufficiently accurate and could for example be based on the residual range R_{res},
- k_{fl} calculated from the fluence based and dose based approaches are given by equations (14) and (15) with standard relative uncertainties of 0.2% and 0.3%, respectively, for the beam energy studied in this work.

Since it has been demonstrated here that non-elastic nuclear interactions are the predominant influence on the fluence correction factors it can also be derived from this work that for plastic phantoms consisting of carbon and hydrogen, like polystyrene or polyethylene, or of carbon, oxygen and hydrogen, like PMMA, the fluence correction factors will be closer to unity or at most as much different from unity as those observed here for pure graphite. The same conclusion can be drawn for most soft tissues.

Acknowledgments

References

Agostinelli S *et al* 2003 GEANT4—a simulation toolkit *Nucl. Instrum. Methods Phys. Res. A* **506** 250–303

Al-Sulaiti L, Palmans H, Thomas R A S, Shipley D and Kacperek A 2010 Water equivalence of A150, aluminium and copper in a low-energy clinical proton beam *Nucl. Instrum. Methods Phys. Res. A* **619** 344–7

Al-Sulaiti L, Shipley D, Thomas R, Owen P, Kacperek A, Regan P H and Palmans H 2012 Water equivalence of some plastic-water phantom materials for clinical proton beam dosimetry *Appl. Radiat. Isot.* **70** 1052–5

Andreo P, Burns D T, Hohlfeld K, Huq M S, Kanai T, Laitano F, Smyth V G and Vynckier S 2000 Absorbed dose determination in external beam radiotherapy: an international code of practice for dosimetry based on standards of absorbed dose to water IAEA *Technical Report Series* 398 (Vienna: IAEA)

Battistoni G, Muraro S, Sala P R, Cerutti F, Ferrari A, Roesler S, Fasso A and Ranft J 2007 The FLUKA code: description and benchmarking *Proc. Hadronic Shower Simulation Workshop 2006 (Fermilab, 6–8 Sept.)* ed M Albrow and R Raja *AIP Conf. Proc.* 896 31–49

Berger M J 1993 Proton Monte Carlo transport program PTRAN *National Institute for Standards and Technology Report* NISTIR 5113 (Gaithersburg, MD: NIST)

Burns J E 1994 Absorbed-dose calibration in high-energy photon beams at the national physical laboratory: conversion procedure *Phys. Med. Biol.* **39** 1555–75

Dementyev A V and Sobolevsky N M 1999 SHIELD—universal Monte Carlo hadron transport code: scope and applications *Radiat. Meas.* **30** 553–57

Duane S, Aldehaybes M, Bailey M, Lee N D, Thomas C G and Palmans H 2012 An absorbed dose calorimeter for IMRT dosimetry *Metrologia* **49** S168–73

DuSautoy A R 1996 The UK primary standard calorimeter for photon beam absorbed dose measurement *Phys. Med. Biol.* **41** 137–51

Ferrari A, Sala P R, Fassò A and Ranft J 2005 FLUKA: a multi-particle transport code CERN 2005-10 INFN /TC 05/11, SLAC-R-773

Gagnebin S, Twerenbold D, Pedroni E, Meer D, Zenklusen S and Bula C 2010 Experimental determination of the absorbed dose to water in a scanned proton beam using a water calorimeter and an ionization chamber beam *Nucl. Instrum. Methods Phys. Res. B* **268** 524–8

Gudowska I, Sobolevsky N, Andreo P, Belkić D and Brahme A 2004 Ion beam transport in tissue-like media using the Monte Carlo code SHIELD-HIT *Phys. Med. Biol.* **49** 1933–58

Hansen D C, Lühr A, Sobolevksy N and Bassler N 2012 Optimizing SHIELD-HIT for carbon ion treatment *Phys. Med. Biol.* **57** 2393–409

ICRU 1993 Stopping powers and ranges for protons and alpha particles *ICRU Report* 49 (Bethesda MD: ICRU)

ICRU 2000 Nuclear data for neutron and proton radiotherapy and for radiation protection dose *ICRU Report* 63 (Bethesda MD: ICRU)

ICRU 2005 Stopping of ions heavier than helium *J. ICRU* **5** 1–253

ICRU 2007 Prescribing, recording, and reporting proton-beam therapy *J. ICRU* **7** 1–210

Jones A Z, Bloch C D, Hall E R, Hashemian R, Klein S B, von Przewoski B, Murray K M and Foster C C 1999 Comparison of Indiana university cyclotron facility Faraday cup proton dosimetry with radiochromic films, a calorimeter, and a calibrated ion chamber *IEEE Trans. Nucl. Sci.* **46** 1762–5

Karger C P, Jäkel O, Palmans H and Kanai T 2010 Dosimetry for ion beam radiotherapy *Phys. Med. Biol.* **55** R193–R234

Krauss A 2007 Application of water calorimetry as absorbed dose to water standard for radiotherapy dosimetry *Proc. Absorbed Dose and Air Kerma Primary Standards Workshop (Paris, France)* (Saclay: LNE-LNHB)

Laitano R F and Rosetti M 2000 Proton stopping powers averaged over beam energy spectra *Phys. Med. Biol.* **45** 3025–43

Lühr A, Hansen D C, Jäkel O, Sobolevsky N and Bassler N 2011a Analytical expressions for water-to-air stopping-power ratios relevant for accurate dosimetry in particle therapy *Phys. Med. Biol.* **56** 2515–33

Lühr A, Hansen D C, Sobolevsky N, Palmans H, Rossomme S and Bassler N 2011b Fluence correction factors and stopping power ratios for clinical ion beams *Acta Oncol.* **50** 797–805

Lühr A, Toftegaard J, Kantemiris I, Hansen D C and Bassler N 2012 Stopping power: the generic library libdEdx and a study of clinically relevant stopping-power ratios for different ions *Int. J. Radiat. Biol.* **88** 209–12

McEwen M R and Duane S 2000 A portable calorimeter for measuring absorbed dose in the radiotherapy clinic *Phys. Med. Biol.* **45** 3675–91

McEwen M R, DuSautoy A R and Williams A J 1998 The calibration of therapy level electron beam ionization chambers in terms of absorbed dose to water *Phys. Med. Biol.* **43** 2503–19

Medin J 2010 Implementation of water calorimetry in a 180 MeV scanned pulsed proton beam including an experimental determination of k_Q for a Farmer chamber *Phys. Med. Biol.* **55** 3287–98

Medin J and Andreo P 1997 Monte Carlo calculated stopping-power ratios, water/air, for clinical proton dosimetry (50–250 MeV) *Phys. Med. Biol.* **42** 89–105

Medin J, Ross C K, Klassen N V, Palmans H, Grusell E and Grindborg J E 2006 Experimental determination of beam quality factors, k_Q, for two types of Farmer chamber in a 10 MV photon and a 175 MeV proton beam *Phys. Med. Biol.* **51** 1503–21

Moyers M F, Coutrakon C B, Ghebremedhin A, Shahnazi K, Koss P and Sanders E 2007 Calibration of a proton beam energy monitor *Med. Phys.* **34** 1952–66

Paganetti H 2002 Nuclear interactions in proton therapy: Dose and relative biological effect distributions originating from primary and secondary particles *Phys. Med. Biol.* **47** 747–64

Paganetti H 2009 Dose to water versus dose to medium in proton beam therapy *Phys. Med. Biol.* **54** 4399–421

Palmans H 2005 McPTRAN.CAVITY and McPTRAN.RZ Monte Carlo codes for the simulation of proton beams and calculation of proton detector perturbation factors *Monte Carlo 2005 Topical Meeting: The Monte Carlo Method—Versatility Unbounded in a Dynamic Computing World* (La Grange Park, IL: American Nuclear Society)

Palmans H, Al-Sulaiti L, Andreo P, Thomas R A S, Shipley D R S, Martinkovic J and Kacperek A 2011 Conversion of dose-to-graphite to dose-to-water in a clinical proton beam *Proc. Int. Symp. on Standards, Applications and Quality Assurance in Medical Radiation Dosimetry (Vienna, 9–12 Nov.)* vol 1 (Vienna, Austria: IAEA) pp 343–55

Palmans H, Bailey M, Duane S, Shipley S and Thomas R 2007 Development of a primary standard level proton calorimeter at NPL *Radiother. Oncol.* **84** (Suppl. 1) S135

Palmans H, Kacperek A and Jäkel O 2009 *Hadron dosimetry Clinical Dosimetry Measurements in Radiotherapy (AAPM 2009 Summer School)* ed D W O Rogers and J Cygler (Madison, WI: Medical Physics Publishing) pp 669–722

Palmans H, Seuntjens J, Verhaegen F, Denis J-M, Vynckier S and Thierens H 1996 Water calorimetry and ionization chamber dosimetry in an 85-MeV clinical proton beam *Med. Phys.* **23** 643–50

Palmans H, Symons J E, Denis J M, de Kock E A, Jones D T and Vynckier S 2002 Fluence correction factors in plastic phantoms for clinical proton beams *Phys. Med. Biol.* **47** 3055–71

Palmans H, Thomas R, Simon M, Duane S, Kacperek A, DuSautoy A and Verhaegen F 2004 A small-body portable graphite calorimeter for dosimetry in low-energy clinical proton beams *Phys. Med. Biol.* **49** 3737–49

Palmans H and Verhaegen F 1997 Calculated depth dose distributions for proton beams in some low-Z materials *Phys. Med. Biol.* **42** 1175–83

Palmans H and Verhaegen F 2005 Assigning nonelastic nuclear interaction cross sections to Hounsfield units for Monte Carlo treatment planning of proton beams *Phys. Med. Biol.* **50** 991–1000

Palmans H *et al* 2013 Fluence correction factors for graphite calorimetry in a low-energy clinical proton beam: II. Experiment *Phys. Med. Biol.* submitted

Pelowitz D 2005 *MCNPX User's Manual LANL Report* LA-CP-05-369 (Los Alamos, NM: Los Alamos National Laboratory)

Reynaert N, Palmans H, Jeraj R and Thierens H 2002 Parameter dependence of the MCNP electron transport in determining dose distributions *Med. Phys.* **29** 2446–54

Rossomme S, Palmans H, Shipley D, Thomas R, Romano F, Bertrand D and Vynckier S 2013 Fluence correction factors for graphite calorimetry in an 80 MeV/n carbon ion beam *Phys. Med. Biol.* submitted

Sakama M, Kanai T, Fukumura A and Abe K 2009 Evaluation of w values for carbon beams in air, using a graphite calorimeter *Phys. Med. Biol.* **54** 1111–30

Sander T, Duane S, Lee N D, Thomas C G, Owen P J, Bailey M and Palmans H 2012 NPL's new absorbed dose standard for the calibration of HDR ^{192}Ir brachytherapy sources *Metrologia* **49** S184–8

Sarfehnia A, Clasie B, Chung E, Lu H M, Flanz J, Cascio E, Engelsman M, Paganetti H and Seuntjens J 2010 Direct absorbed dose to water determination based on water calorimetry in scanning proton beam delivery *Med. Phys.* **37** 3541–50

Sassowsky M and Pedroni E 2005 On the feasibility of water calorimetry with scanned proton radiation *Phys. Med. Biol.* **50** 5381–400

Schneider U, Pemler P, Besserer J, Dellert M, Moosburger M, de Boer J, Pedroni E and Boehringer T 2002 The water equivalence of solid materials used for dosimetry with small proton beams *Med. Phys.* **29** 2946–51

Schulz R J, Verhey L J, Huq M S and Venkataramanan N 1992 Water calorimeter dosimetry for 160 MeV protons *Phys. Med. Biol.* **37** 947–53

Siebers J V, Vatnitsky S M, Miller D W and Moyers M F 1995 Deduction of the air w value in a therapeutic proton beam *Phys. Med. Biol.* **40** 1339–56

Sigmund P, Schinner A and Paul H 2009 Errata and addenda for 'Stopping of ions heavier than helium' *ICRU Report* 73 (Bethesda MD: ICRU) (http://icru.org/images/pdf/errata_and_addenda.pdf)